A Finite Element Method with Nonlocal Boundary Conditions for the Helmholtz Equation with Complex Wavenumber in Stratified Waveguides

D. A. Mitsoudis and M. Plexousakis
Department of Applied Mathematics, University of Crete,
71409 Heraklion, Greece
e-mail: dmits@tem.uoc.gr, plex@tem.uoc.gr
and
Institute of Applied and Computational Mathematics,
FO.R.T.H., P.O. Box 1527, 71110 Heraklion, Greece.

Abstract

A finite element method for solving the Helmholtz equation with a complex wavenumber in an axially symmetric stratified waveguide is presented. We use a standard Galerkin discretization coupled to nonlocal nonreflecting boundary conditions posed on two artificial boundaries near and far from the source. The proposed method is implemented in a Fortran code called CFENL and validated by comparing its results with those of COUPLE.

PACS no. 43.20.Bi, 43.30.Gv, 43.30.Bp

Short title: Finite elements for Helmholtz equation with complex wavenumber.

1 Introduction.

In the area of underwater acoustics, the Helmholtz equation models the propagation and backscattering of the sound field generated by a continuous time-harmonic signal. Frequently, the physical domain is assumed to be an axially symmetric stratified waveguide consisting of several fluid layers overlying a rigid bottom. Here we shall consider, for simplicity, two layers; the upper one representing the sea water, while the lower one a fluid sediment layer, where attenuation is included. The acoustic pressure field generated by a time-harmonic point source of frequency f, placed in the water column at a depth

equal to $z_{\rm s}$, and range $r = 0$, satisfies in each layer the Helmholtz equation, *cf.* [1],

$$u_{rr} + \frac{1}{r}\, u_r + u_{zz} + k^2\, u = -\frac{1}{2\pi r}\, \delta(r)\, \delta(z - z_{\rm s}), \tag{1}$$

where $k = k(r,z) := \omega / c\,(r,z)$ is the wavenumber, ω is the circular frequency and $c = c(r,z)$ is the sound speed which is equal to $c_{\rm w}(r,z)$ in the water layer and $c_{\rm s}(r,z)$ in the sediment. In each layer the density of the medium is assumed to be constant and equal to $\rho_{\rm w}$ in the water layer and $\rho_{\rm s}$ in the sediment ($\rho_{\rm s} > \rho_{\rm w}$). In order to allow for attenuation in the sediment layer, an imaginary part may be added in the wavenumber. Specifically, we assume that

$$k = \begin{cases} k_{\rm w}, & \text{in the water layer} \\ k_{\rm s}(1 + {\rm i}\,\varepsilon), & \text{in the sediment layer} \end{cases}, \tag{2}$$

with $k_{\rm w} = \omega / c_{\rm w}(r,z)$, $k_{\rm s} = \omega / c_{\rm s}(r,z)$ and $\varepsilon = a^{(\lambda)} / (40\pi \log_{10} {\rm e})$, where $a^{(\lambda)}$ is the attenuation of the medium in units of dB per wavelength.

The partial differential equation (1) is supplemented with a pressure-release surface condition $u = 0$, a Neumann bottom boundary condition $\frac{\partial u}{\partial n} = 0$, the usual transmission conditions across the interface, and an outgoing radiation condition as $r \to \infty$.

Various semi-analytical and numerical methods have been proposed for solving this problem, see e.g. [1] and [2]. Of course, the appropriate method is often indicated by the particular characteristics of the problem under consideration. For example, if the ocean environment exhibits strong range-dependence or complicated sea-bed topography, then, naturally, one should turn its attention to a direct numerical method, such as a finite element method. However, in order to use a direct numerical method one has to take into account the following two issues: (a) The physical domain is unbounded, therefore it has to be truncated and an equivalent problem must be posed in the bounded computational domain. (b) Solving the Helmholtz equation numerically may be computationally expensive; let us recall here the well-known fact that the error in the finite element solution increases with the frequency and in order to keep the error bounded as the frequency increases the discretization parameter should be appropriately adjusted with a reference wavenumber, see e.g. the book by Ihlenburg, [3], and the references therein. Having these in mind, a standard Galerkin/finite element discretization has been proposed in [4], coupled to nonlocal nonreflecting boundary conditions posed on two artificial boundaries near the source and far from the source. The waveguide, see Fig. 1, was assumed to consist of three parts: (a) A near-field bounded subdomain $\Omega^{\rm N} := \Omega^{\rm N}_{\rm w} \cup \Omega^{\rm N}_{\rm s}$ (for $0 \le r \le r^{\rm N}$), where the interface and the bottom were horizontal at constant depths $z = d^{\rm N}$ and $z = D^{\rm N}$, respectively, (b) an intermediate bounded subdomain Ω (for $r^{\rm N} < r < r^{\rm F}$), containing the variable interface and bottom, and (c) a far-field, semi-infinite subdomain $\Omega^{\rm F} := \Omega^{\rm F}_{\rm w} \cup \Omega^{\rm F}_{\rm s}$ (for $r \ge r^{\rm F}$),

where the interface and the bottom were also horizontal at constant depths $z = d^{\mathrm{F}}$ and $z = D^{\mathrm{F}}$, respectively.

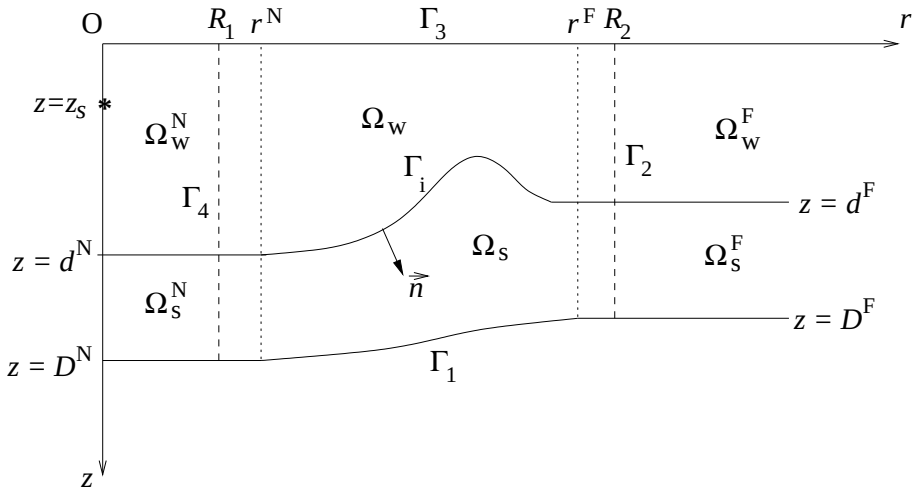

Figure 1: The waveguide under consideration and basic notation.

In this way the finite element method was applied just to the 'difficult' intermediate part of the waveguide, while the effect of the source and the radiation condition were incorporated into the boundary conditions posed on the artificial boundaries, see [4] and the references therein. This method was implemented in a code called FENL^2, which was validated by comparing its outcome with COUPLE, [5], a widely used code based on a coupled mode method by Evans, [6]. Nevertheless, in [4] there was no attenuation included in the two layers.

In the present note we extend this method to include an attenuating fluid sediment layer, by introducing a *complex wavenumber*, see Eq. (2), and we implement it in a code referred to as CFENL in the sequel. In the next section we outline briefly the basic features of the method and, also, the extensions and developments that were done in CFENL with respect to FENL^2. In Section 3 we present results of a numerical experiment that we performed with the code in an underwater waveguide simulating a sinusoidal interface environment. In order to validate the code we compared our results with those of COUPLE and found them to be in excellent agreement. In order to assess the performance of our method we also show results in the case where a rigid obstacle is placed in the waveguide. We close with some concluding remarks.

2 The finite element method.

With reference to Fig. 1 we introduce two artificial boundaries, one near the source at a range $r = R_1$, where $0 < R_1 < r^{\mathrm{N}}$, and another far from the source at a range $r = R_2$, where $R_2 > r^{\mathrm{F}}$. We shall denote by Γ_4 and Γ_2 the near- and the far-field artificial boundaries, respectively. We also let Γ_1,

Γ_3, and Γ_i denote the parts of the bottom, the surface and the interface, respectively, lying between the cylinders $r = R_1$ and $r = R_2$. Therefore, our computational domain, denoted by Ω, will be the one enclosed by $\Gamma_1 \cup \Gamma_2 \cup \Gamma_3 \cup \Gamma_4 =: \partial\Omega$. Then, instead of solving the original problem, we seek a complex-valued function $u(r,z)$, $(r,z) \in \overline{\Omega}$, such that

$$\Delta u + k^2(r,z)u = 0 \ \text{ in } \Omega_\mathrm{w} \cup \Omega_\mathrm{s}, \tag{3}$$

$$u\,|_{\Gamma_\mathrm{i}-} = u\,|_{\Gamma_\mathrm{i}+}, \tag{4}$$

$$\frac{1}{\rho_\mathrm{w}} \frac{\partial u}{\partial n}\bigg|_{\Gamma_\mathrm{i}-} = \frac{1}{\rho_\mathrm{s}} \frac{\partial u}{\partial n}\bigg|_{\Gamma_\mathrm{i}+}, \tag{5}$$

$$\frac{\partial u}{\partial n} = 0 \text{ on } \Gamma_1, \tag{6}$$

$$\frac{\partial u}{\partial r} = T(u) \text{ on } \Gamma_2, \tag{7}$$

$$u = 0 \text{ on } \Gamma_3, \tag{8}$$

$$\frac{\partial u}{\partial r} = R(u) + S \text{ on } \Gamma_4. \tag{9}$$

Equation (7) is a classical DtN 'transparent' nonlocal boundary condition associated with the exterior acoustic field, and the operator T is defined as

$$T(u)(z) := \sum_{n=1}^{\infty} b_n(u)\, Z_n^\mathrm{F}(z), \tag{10}$$

where

$$b_n(u) = \sqrt{\lambda_n^\mathrm{F}}\, \frac{H_0^{(1)'}(\sqrt{\lambda_n^\mathrm{F}} R_2)}{H_0^{(1)}(\sqrt{\lambda_n^\mathrm{F}} R_2)} \left(u(R_2,\cdot), \overline{Z_n^\mathrm{F}}\right)_{L^2_\rho(0,D^\mathrm{F})},$$

and $H_0^{(1)}$ is the Hankel function of the first kind and order zero, while the prime denotes differentiation with respect to its argument.

Similarly, (9) is a nonhomogeneous DtN-type boundary condition relating the fields in Ω and in the near-field region Ω^N, where

$$R(u)(z) := \sum_{n=1}^{\infty} a_n(u)\, Z_n^\mathrm{N}(z), \tag{11}$$

$$S(z) := -\frac{1}{2\pi\rho_\mathrm{w} R_1} \sum_{n=1}^{\infty} \frac{1}{J_0(\sqrt{\lambda_n^\mathrm{N}} R_1)}\, Z_n^\mathrm{N}(z_\mathrm{s})\, Z_n^\mathrm{N}(z), \tag{12}$$

and

$$a_n(u) = \sqrt{\lambda_n^\mathrm{N}}\, \frac{J_0'(\sqrt{\lambda_n^\mathrm{N}} R_1)}{J_0(\sqrt{\lambda_n^\mathrm{N}} R_1)} \left(u(R_1,\cdot), \overline{Z_n^\mathrm{N}}\right)_{L^2_\rho(0,D^\mathrm{N})},$$

with J_0 being the Bessel function of order zero.

Here $(w,u)_{L^2_\rho(0,D^*)} := \int_0^{d^*} w\,\overline{u}\,dz + \rho \int_{d^*}^{D^*} w\,\overline{u}\,dz$, where $\rho := \rho_\mathrm{w}/\rho_\mathrm{s}$, and in place of the asterisk $*$, we read N in the near-field region Ω^N, and F in the far-field region Ω^F. $\{\lambda_n^*, Z_n^*(z)\}$, $n = 1, 2, \ldots$, denote the (complex) eigenvalues and the corresponding eigenfunctions of the two-point vertical eigenvalue problem $L^*v := \frac{d^2v}{dz^2} + \left[(k^*(z))^2 - \lambda_n^*\right] v = 0$ in $[0, d^*) \cup (d^*, D^*]$, with $v(0) = 0$, $v(d^*-) = v(d^*+)$,

$\frac{1}{\rho_w}\frac{dv}{dz}(d^*-) = \frac{1}{\rho_s}\frac{dv}{dz}(d^*+)$, and $\frac{dv}{dz}(D^*) = 0$. We would like to note that (10)–(12) are of the same form as in the case of a real wavenumber, *cf.* [4], but now the eigenvalues and the corresponding eigenvectors are complex and the Hankel and Bessel functions appearing in the coefficients a_n, b_n, and in the function S, are functions of a complex argument. Note, also, that since k^* is complex the operator L^* is not selfadjoint, in contrast with the case of a real wavenumber. Nevertheless, the sequence of the eigenfunctions $\{Z_n^*\}_{n=1,2,\ldots}$ and the sequence of their complex conjugates $\{\overline{Z_n^*}\}_{n=1,2,\ldots}$ form, under certain hypotheses, a complete biorthogonal system in $L^2_\rho(0, D^*)$, which we assume to be normalized with respect to the $(\cdot,\cdot)_{L^2_\rho(0,D^*)}$ inner product, *i.e.*, $(Z_m^*, \overline{Z_n^*})_{L^2_\rho(0,D^*)} = \delta_{mn}$, where δ_{mn} is the Kronecker delta. For details, we refer to Evans, [6], and the references therein. We assume that the eigenvalues λ_n^* are ordered with decreasing real parts. By analogy with the case of a real wavenumber we shall refer to the modes corresponding to eigenvalues with positive real part as the *propagating* modes and to the rest as the *evanescent* modes.

We discretize the boundary-value problem (3)–(9) using the standard Galerkin/finite element method with continuous, piecewise linear functions on a triangulation of Ω with triangles of maximum sidelength h. The nonlocal boundary conditions (9) and (7) are treated as generalized natural boundary conditions on Γ_4 and Γ_2, respectively, and are approximated by their discrete analogues evaluated as finite sums including all the propagating and the most significant of the evanescent modes. Specifically, we shall denote by L^{N} the number of terms retained in the series (11), (12), and L^{F} the number of terms retained in the series (10).

2.1 Implementation issues.

We implemented the basic finite element module in a Fortran code, referred to as CFENL in the sequel. This code modifies and extends an existing code called FENL^2, [4], in order to handle an attenuating sediment layer. FENL^2 in turn, was based on a code called FENL, [7], and its main novelty with respect to FENL was the use of a nonlocal near-field boundary condition incorporating the effect of the point source. For the necessity and importance of this kind of treatment for the near-field boundary we refer to [4] and [8].

Here we shall briefly describe some of the the aspects in which CFENL differs from FENL^2.

Triangulation of the domain. To triangulate the domain Ω we now use the two-dimensional Delaunay triangulator called Triangle, developed by J. Shewchuk (*cf.* `http://www.cs.cmu.edu/~quake/triangle.htm`). This allowed us to produce larger grids than in FENL^2 and to handle larger domains and/or higher frequencies.

The eigenvalue problems. In order to construct the nonlocal conditions (7) and (9) we have to solve the associated vertical eigenvalue problems on Γ_2 and Γ_4, respectively. This is performed with the aid of a finite element method. In what follows we suppress the symbol $*$.

The interval $[0, D] := [0, d] \cup [d, D]$ is divided in M subintervals arranging so that (the interface) d is a node. We define the finite element space $X_h = \Big\{\chi : \chi \in C([0, D]),\ \chi\,|_{[z_i, z_{i+1}]} \in \mathbb{P}_1,\ 0 \le i \le M-1,\ \chi(0) = 0\Big\}$, and we seek eigenvalues $\lambda_h \in \mathbb{C}$ and corresponding eigenfunctions $Z_h \in X_h$ of the discrete problem

$$-(Z_h', \chi')_{L^2_\rho(0,D)} + (k^2 Z_h, \chi)_{L^2_\rho(0,D)} = \lambda_h (Z_h, \chi)_{L^2_\rho(0,D)}, \tag{13}$$

for all $\chi \in X_h$. Let $\{\chi_i\}_{i=1}^M$ denote the usual (nodal) basis of X_h. Then, writing $Z_h = \sum_{j=1}^M f_j \chi_j$ and setting $\chi = \chi_i$ in (13), for $i = 1, \ldots, M$, we end up with the following generalized algebraic eigenvalue problem

$$(-S + Q)\boldsymbol{f} = \lambda_h G \boldsymbol{f}, \quad \boldsymbol{f} = (f_1, \ldots, f_M)^T, \tag{14}$$

where S and G are the (tridiagonal real symmetric) stiffness and mass matrices, respectively, with entries $S_{ij} = (\chi_j', \chi_i')_{L^2_\rho(0,D)}$, $G_{ij} = (\chi_j, \chi_i)_{L^2_\rho(0,D)}$, and Q is the tridiagonal complex symmetric matrix with entries $Q_{ij} = (k^2 \chi_j, \chi_i)_{L^2_\rho(0,D)}$. Then (14) may be written as

$$A\boldsymbol{f} = \lambda_h \boldsymbol{f}, \text{ where } A := G^{-1}(-S + Q).$$

To compute A we solve the matrix equation $GA = -S + Q$, with standard routines from the freely available linear algebra package LAPACK (*cf.* `http://www.netlib.org/lapack/`). Then, we use the LAPACK routine `zgeev` to compute the eigenvalues and eigenvectors of the matrix A. Although this routine is designed for full non-symmetric complex matrices and does not take any advantage of the sparseness or the symmetry of the matrix A, we have decided to use it for two reasons: First, the vertical eigenvalue problem need only be solved twice, and is one-dimensional, therefore the cost of using `zgeev` is not large and, second, it is a robust routine.

Finally, to compute the values of the special functions of complex arguments involved, we used subroutines of the freely available AMOS library (*cf.* `http://www.netlib.org/amos/`), developed by D. E. Amos, [9].

3 A Numerical experiment.

We have experimented with our code in various underwater environments and in all cases we have compared our results with those of COUPLE and found them to be in excellent agreement. Here we present the results for a test case simulating a sinusoidal interface given by the function

$$g(r) = \begin{cases} 75 - 25\cos\frac{\pi(r-500)}{50} & , \text{ for } 300 < r < 700, \\ 50 & , \text{ elsewhere.} \end{cases}$$

(All distances are in meters.) A rigid horizontal bottom is located at a depth of 150 m. The water column and the sediment layer are considered to be homogeneous with parameters $c_{\rm w} = 1500$ m/sec, $\rho_{\rm w} = 1.0$ g/cm^3 and $c_{\rm s} = 1700$ m/sec, $\rho_{\rm s} = 1.5$ g/cm^3, respectively. In the sediment layer an attenuation coefficient $a^{(\lambda)}$ of 0.5 dB per wavelength is assumed. The point source of frequency 25 Hz is placed at a depth equal to 25 m. For this frequency five modes propagate at both artificial boundaries. In order to validate our results we also ran COUPLE in this environment, by approximating the sinusoidal interface (for $300 \le r \le 700$) with 1000 staircase steps. The number of contributing modes was taken equal to 30 and the rigid bottom was simulated, as proposed in [10], by assuming very large values for the density (10^5 g/cm^3) and the sound speed (10^{10} m/sec) in the terminating bottom layer used by COUPLE.

In all CFENL runs the near-field boundary condition was posed at $R_1 = 250$ m, while the far-field one was posed at $R_2 = 750$ m, and $L^{\rm N} = 15$ and $L^{\rm F} = 5$ modes were employed in the near- and the far-field boundary conditions, respectively. We have checked that for the values of the parameters referred above the codes have converged (within the line thickness in one-dimensional horizontal and vertical transmission loss plots).

We ran CFENL with three grids named S1, S2 and S3 from the coarser to the finer. In order to quantify the discrepancies between the results of the two codes we measure a relative ℓ_2–discrepancy, at a receiver depth $z = z_{rd}$, defined as the quantity $\left(\frac{1}{N_s} \frac{\sum_{i=1}^{N_s} |u_c(r_i,z_{rd}) - u_h(r_i,z_{rd})|^2}{\sum_{i=1}^{N_s} |u_c(r_i,z_{rd})|^2} \right)^{1/2}$, where u_c denotes the approximate solution obtained by COUPLE, u_h is the approximation obtained by CFENL and r_i, $i = 1, \ldots, N_s$, is the set of the sampling points in the range interval $[250, 750]$. In practice, the CFENL field values were computed at the points (r_i, z_{rd}), $i = 1, \ldots, N_s$, determined by COUPLE, by linear interpolation. Table 1 summarizes the parameters of the grids that we used, the value of two parameters, denoted by $\xi_{\rm w}$ and $\xi_{\rm s}$, which measure the number of average size meshlengths contained in a wavelength in the water, and the sediment, for constant sound speeds $c_{\rm w} = 1500$ m/sec and $c_{\rm s} = 1700$ m/sec, respectively, as well as, the relative ℓ_2–discrepancy at receiver depths RD = 25, 75 and 125 m.

Grid	# of Elements	# of Nodes	$\xi_{\rm w}$	$\xi_{\rm s}$	Relative ℓ_2-discrepancy RD=25 m	RD=75 m	RD=125 m
S1	38789	19724	31	35	1.5537e-03	2.0288e-03	2.5935e-03
S2	78018	39489	43	49	9.4380e-04	1.1706e-03	1.3538e-03
S3	116916	59039	53	60	8.1439e-04	9.3840e-04	1.0250e-03

Table 1: Mesh parameters for the CFENL runs and relative ℓ_2 field discrepancies between CFENL and COUPLE.

In all runs we solved the linear system using the double precision complex version of the routine CPL from QMRPACK software package, [11], which is based on the coupled two-term recurrence Lanczos process with look-ahead, [12]. From the built-in preconditioners of QMRPACK we have experimented mainly with two-sided SSOR and two-sided ILUT. For the runs with the Grids S1 and S2, CPL was preconditioned with two-sided SSOR with parameter $\omega = 1.2$. Then, 970 iterations and 24 secs of CPU time and 1386 iterations and 71 secs of CPU time, respectively, were needed for convergence. For the Grid S3, the solver CPL preconditioned with two-sided ILUT, with fill-in=5 and tolerance=10^{-3}, needed 688 iterations and 344 secs to converge.

Finally, in order to give some idea of the capabilities of the finite element method, we placed a rigid (axisymmetric) ellipsoidal object with a major axis of 60 m and a minor axis of 20 m, centered at the point $r = 550$ m, $z = 40$ m. In terms of wavelengths this object is one wavelength long, assuming a reference sound speed of 1500 m/sec in the water. In the two first rows of Figure 2 the two-dimensional transmission loss plots produced by COUPLE and CFENL results, respectively, confirm the excellent agreement between the results of the two codes in the absence of the ellipsoidal obstacle. The CFENL results have been obtained with the Grid S3. In the third row, the disturbances due to the presence of the obstacle are depicted.

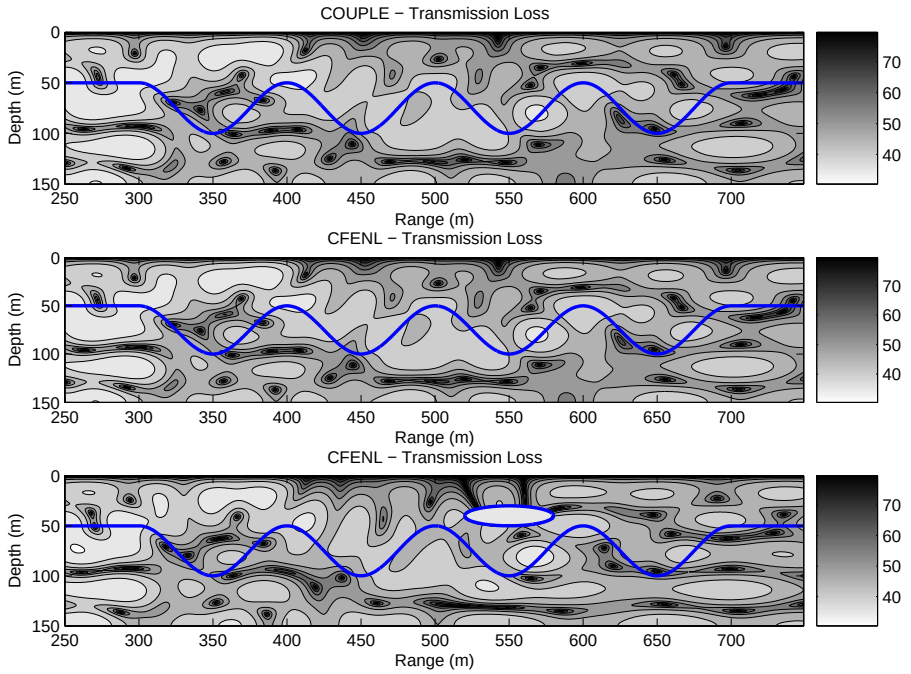

Figure 2: Sinusoidal interface. Transmission loss. COUPLE and CFENL, f=25 Hz.

The situation becomes clearer in the superimposed one-dimensional transmission loss plot, for receiver depth RD = 25 m, of Figure 3. The solid line corresponding to COUPLE results can hardly be distinguished by the dashed-dotted line corresponding to CFENL results when there is no object. The

dashed line corresponds to CFENL results in the presence of the obstacle, and one may immediately confirm discrepancies of few dB's between the case with and without the obstacle.

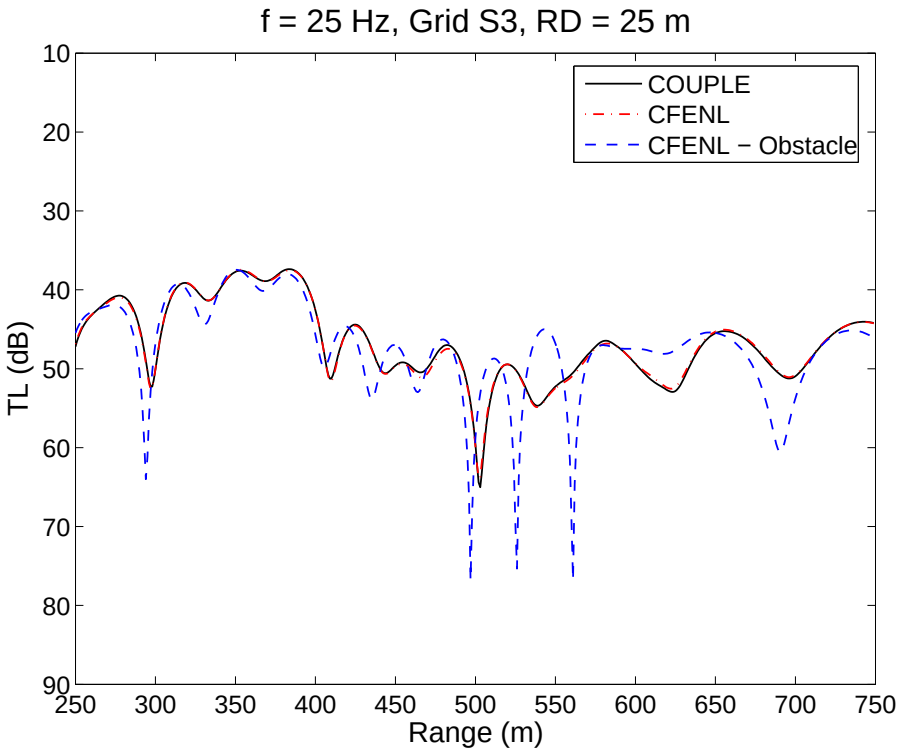

Figure 3: Comparison between COUPLE and CFENL in the absence of the obstacle and the effect of its presence.

4 Concluding Remarks.

A standard Galerkin/finite element method coupled to nonlocal boundary conditions posed on two artificial boundaries, near and far from the source, has been presented for the Helmholtz equation with a complex wavenumber in an axisymmetric stratified waveguide. The method has been implemented in a Fortran code called CFENL and validated by comparing its results to those obtained by COUPLE. Results have been presented for a complicated environment with a sinusoidal interface and a rigid obstacle.

Ongoing work includes a systematic study of the influence of the various parameters, e.g. the position of the artificial boundaries and the number of modes employed in the nonlocal boundary conditions, on the accuracy of the solution. It is in our plans to experiment with other linear system solvers and preconditioners in order to reduce the calculation times, and also replacing the idealized rigid bottom assumption by a more realistic one.

Acknowledgement

The authors express their sincerest thanks to three anonymous referees for their useful comments and suggestions.

References

[1] F. B. Jensen, W. A. Kuperman, M. B. Porter, H. Schmidt, *Computational Ocean Acoustics*, (American Institute of Physics, New York, 1994).

[2] M. J. Buckingham, Ocean-acoustic propagation models, *J. Acoustique*, **3** (1992) 223–287.

[3] F. Ihlenburg, *Finite Element Analysis of Acoustic Scattering*, Springer, 1998.

[4] D. A. Mitsoudis, Near- and far-field boundary conditions for a finite element method for the Helmholtz equation in axisymmetric problems of underwater acoustics, *Acta Acustica united with Acustica*, **93** (2007) 888–898.

[5] R. B. Evans, COUPLE: a user's manual, NORDA TN–332, 1986.

[6] R. B. Evans, A coupled mode solution for the acoustic propagation in a waveguide with stepwise depth variations of a penetrable bottom, *J. Acoust. Soc. Am.*, **74** (1983) 188–195.

[7] N. A. Kampanis, V. A. Dougalis, A finite element code for the numerical solution of the Helmholtz equation in axially symmetric waveguides with interfaces, *J. Comp. Acoustics*, **7** (1999) 83–110.

[8] G. A. Athanassoulis, K. A. Belibassakis, D. A. Mitsoudis, N. A. Kampanis, V. A. Dougalis, Coupled mode and finite element solutions of underwater sound propagation problems in stratified environments, *J. Comp. Acoustics*, **16** (2008) 83–116.

[9] D. E. Amos, A Portable Package for Bessel Functions of a Complex Argument and Nonnegative Order, *ACM Trans. Math. Software*, **12** (1986) 265–273.

[10] F. B. Jensen, C. M. Ferla, Numerical solution of range-dependent benchmark problems in ocean acoustics, *J. Acoust. Soc. Am.*, **87** (1990) 1499–1510.

[11] R. W. Freund, N. M. Nachtigal, QMRPACK: A package of QMR Algorithms, *ACM Trans. Math. Software*, **22** (1996) 46–77.

[12] R. W. Freund, N. M. Nachtigal, An implementation of the QMR method based on coupled two-term recurrences, *SIAM J. Sci. Comput.*, **15** (1994) 313–337.